A Comparative Study of the Oxidation Behavior of Hot-Rolled Steel established from Medium and Thin Slabs oxidized in 20% H_2O-N_2 at 600-900°C

Seksan Singthanu
Program in Industrial Management Engineering, Faculty of Industrial Technology, Rajabhat Rajanagarindra University, Thailand
ssc.sek9@gmail.com

Thanasak Nilsonthi
High Temperature Corrosion Research Centre and Department of Materials and Production Technology Engineering, Faculty of Engineering, King Mongkut's University of Technology, Thailand
thanasak.n@eng.kmutnb.ac.th (corresponding author)

Received: 5 July 2023 | Revised: 27 November 2023 | Accepted: 29 November 2023

 DOI: https://doi.org/10.48084/etasr.6168

ABSTRACT

This study focuses on the oxidation behavior of oxide scale on hot-rolled steel from a Thailand steel industry. Hot-rolled steel established from the medium and thin slabs was studied. The oxidation behavior was conducted in a horizontal furnace with 20% H2O-N_2 to simulate steel oxidation during the hot rolling line. The scale was formed at a temperature range of 600-900°C for 30, 60, and 90 min. The scale morphology can be seen via Scanning Electron Microscope (SEM-EDS). The oxide phase was investigated via X-Ray Diffraction (XRD). The results show that iron oxides such as hematite (Fe_2O_3) and magnetite (Fe_3O_4) were produced on the studied steel. The oxidation behavior of the studied steel was followed by a parabolic law. The mass gain increased with increasing temperatures. The steel established from a medium slab exhibited a lower oxidation rate than the steel established from a thin slab. The reason for this could be the high amount of oxide containing silicon at the steel-scale interface, which promoted the oxidation resistance of the steel established from the medium slab. The influence of different slab types and its alloying elements was studied to comprehend the oxidation behavior. As a result, the alloying element in the hot-rolled steel was controlled in the design process.

Keywords-oxidation; water vapor; hot-rolled steel; medium slab; thin slab

I. INTRODUCTION

In Thailand, recycling steel or producing it in Electric Arc Furnaces (EAFs) rather than Blast Furnaces (BFs) are the primary methods of manufacturing steel. Steel is primarily manufactured using scraps as basic materials. The thickness of the slab produced by the furnaces could be used to classify them, i.e. the conventional slab manufactured by the BF process typically has a thickness of about 200 mm. In the EAF process, the scraps can make a medium slab, when the thickness is ca. 80 to 100 mm or a thin slab when the thickness is ca. 50 mm [1, 2]. Metallic iron is the majority constituent of the slab produced via the EAF process. Si, Cu, and Sn as contaminants in scraps are challenging to oxidize and remove through the steelmaking process. Furthermore, Si may be present in steel within a range of 0.03 to 0.25 wt.% as a deoxidizer element during the steelmaking process, while the acceptable range for copper content is between 0.12 and 0.20 wt.% [1]. Oxide scale always accumulates on the hot-rolled steel surface during the rolling process [3-5]. Hematite (Fe_2O_3), magnetite (Fe_3O_4), and wustite (FeO) are the major layers found in the oxide scales that form on the steel surface [3-8]. The morphologies of the oxide scales differ according to the alloying elements [9-14] and oxidizing atmosphere [15-19]. Stainless steel or alloy steel models have been used in many studies, but there are a limited number of studies regarding hot-rolled steel [20-25]. There are some studies on the effect of silicon alloys on oxide formation [26-30]. Some research has been conducted on the effects of the presence of water vapors on the oxidation behavior of low-carbon steel [31-33]. Studying the oxidation behavior of hot-rolled steel established from medium and thin slabs is the purpose of the current paper. In particular, Si plays an important role in alloying and oxidation behavior.

II. MATERIALS AND METHODS

Hot-rolled low-carbon steel with silicon concentrations of 0.173 and 0.242 wt.% is the focus of this study. The specimen is cut from steel strips made from slabs that were produced using the electric arc furnace process, manufactured by the G Steel Public Company Limited. The specimen contained a higher Si content steel established from a medium slab with a final thickness of 2.2 mm after hot rolling and a lower Si content steel established from a thin slab with a final thickness of 2.4 mm after hot rolling. These steels had comparable finishing and coiling temperatures of 880 °C and 580 °C, respectively. Table I lists the chemical compositions of the studied steels.

TABLE I. CHEMICAL COMPOSITIONS (WT.%) OF THE STUDIED HOT-ROLLED STEELS

Steel established from	C	Si	Cu	Mn	P	S	Fe
Medium slab	0.067	0.242	0.199	0.387	0.007	0.008	Bal.
Thin slab	0.057	0.173	0.195	0.376	0.020	0.005	Bal.

SEM (Quanta 450) observations of the scale morphology and cross-section were conducted to study the oxide scales. EDS (X-Max) is an energy-dispersive X-ray spectroscopy technique that uses element analysis. Using the XRD D8 Advance technique, the Cu Kα line (0.15406 nm) with 0.02 degrees/step step size and 0.5 s/step step time is used to identify the phases that occur following the oxidation. The prepared hot-rolled steel has dimensions of 10 mm width, 10 mm length, and 2 mm thickness. Before being exposed to oxidation in the horizontal furnace, the sample was polished to eliminate the oxide scale as received from the hot rolling process. The oxide scale on the sample was grounded to a 1200 grid using SiC papers. Afterward, it was given a final cleaning with alcohol in an ultrasonic machine, dried in air, and then taken instantly to the furnace. The oxidation atmosphere within the furnace consisted of 20% water vapor and 80% nitrogen, for 30, 60, and 90 min at a flow rate of 1.2 L/min at temperatures between 600 and 900°C. In this atmosphere, the temperature control of the heating machine for the water-containing vessel was set at 60°C with a 20°C/min of heating rate applied to the furnace. Once the furnace reached the desired temperature, the sample and water vapor were delivered into it. After the variable time oxidation, nitrogen was fed into the furnace until it has cooled to room temperature. Finally, mass gain was measured by an electronic microbalance.

III. RESULTS AND DISCUSSION

The steel which mainly contained iron was oxidized to form three oxide scales, Fe_2O_3, Fe_3O_4, and FeO. Initially, the oxidation rate was controlled by the oxygen diffusion to the surface reaction. The process rate in this instance remained constant. Through this process, a non-protective porous scale could be formed. The oxidation kinetics corresponds to the linear law:

$$\frac{\Delta m}{A} = k_l \cdot t \quad (1)$$

where Δm is the mass gain (g), A is the surface area (cm^2), k_l is the linear rate constant ($g.cm^{-2}.s^{-1}$), and t as the oxidation time (s).

Finally, the diffusion of iron through the scale controls the oxidation rate. Normally, the steel surface produces a protective non-porous scale. The oxidation rate followed the parabolic law:

$$\left(\frac{\Delta m}{A}\right)^2 = k_p \cdot t \quad (2)$$

where Δm is the mass gain (g), A is the surface area (cm^2), k_p is the parabolic rate constant ($g.cm^{-2}.s^{-1}$), and t is the oxidation time (s).

The process of metal oxidation involved an inward diffusion of electrons through the scale layer, which was accompanied by the transfer of iron cations from the metal toward the oxide-gas interface. Figure 1 shows an illustrated cross-sectional view of a forming oxide scale.

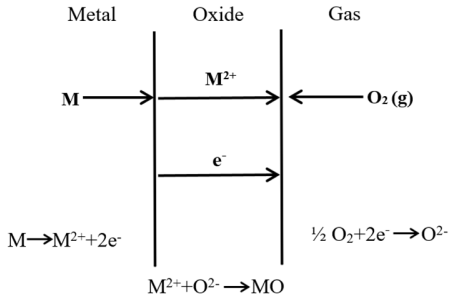

Fig. 1. Ion and electron transport on a growing oxide scale.

XRD was applied to the hot-rolled steel. Peaks of hematite and magnetite were clearly detected, as shown in Figure 2. The morphology of the oxide scale on both specimens under simulated oxidation is shown in Figure 3. An oxide layer was formed when steel was oxidized in 20%H_2O-N_2 at 900°C for 90 min. The interfacial layer exhibits Fe, O, and C peaks as well as a Si peak when using Energy Dispersive Spectroscopy (EDS). The scale on steel established from a medium slab was thinner than that established from a thin slab, possibly due to the higher oxide containing Si or fayalite, present at the scale-steel interface which revealed a decreased scaling rate of the former steel.

The oxygen generated from water vapor dissociation oxidizes the iron. The oxidation of iron and oxygen should be followed in the high oxygen activity condition. The classic three-layered oxide scale should follow this route:

$$H_2O \rightarrow H_2 + 1/2O_2 \quad (3)$$

$$Fe \rightarrow Fe_{1-y}O \rightarrow Fe_3O_4 \rightarrow Fe_2O_3 \quad (4)$$

From thermodynamic calculations, the dissociation of 20% water vapor was finally accomplished. The partial pressure of the oxygen in the reactor was much higher than its partial pressure in equilibrium when forming the oxides. In the gas

phase, the partial pressure of oxygen was 1.90×10^{-5} atm at 900 °C, which was sufficiently higher than the oxygen partial pressure in equilibrium with wustite/magnetite/hematite formations, which was 2.51×10^{-17} atm, 1.80×10^{-15} atm, and 1.10×10^{-8} atm respectively. It can be confirmed that the iron oxides detected in this work can be thermodynamically formed under the studied conditions. Hydrogen atoms in the form of hydrogen gas (H_2) can be dissolved in the oxide. In a static mode, the hydrogen dissolved in the oxide was formed by assuming that the partial pressures of the gases in the reactor were constant. The thermodynamic information of the oxidation reaction was calculated using the data compiled from [34, 35] and the result is shown in Table II.

TABLE II. THERMODYNAMIC INFORMATION ON OXIDATION REACTIONS

Reaction	$G_{900°C}$ (J)	P_{H_2O}/P_{H_2}	P_{O_2} (atm)
$H_2O \rightarrow H_2 + 1/2O_2$	181,720	523,560	1.90×10^{-5}
$2Fe_3O_4 + H_2O \rightarrow 3Fe_2O_3 + H_2$	92,394	13,018	1.10×10^{-8}
$3FeO + H_2O \rightarrow Fe_3O_4 + H_2$	16,202	5.26	1.80×10^{-15}
$H_2O + Fe \rightarrow FeO + H_2$	-4,505	0.62	2.51×10^{-17}

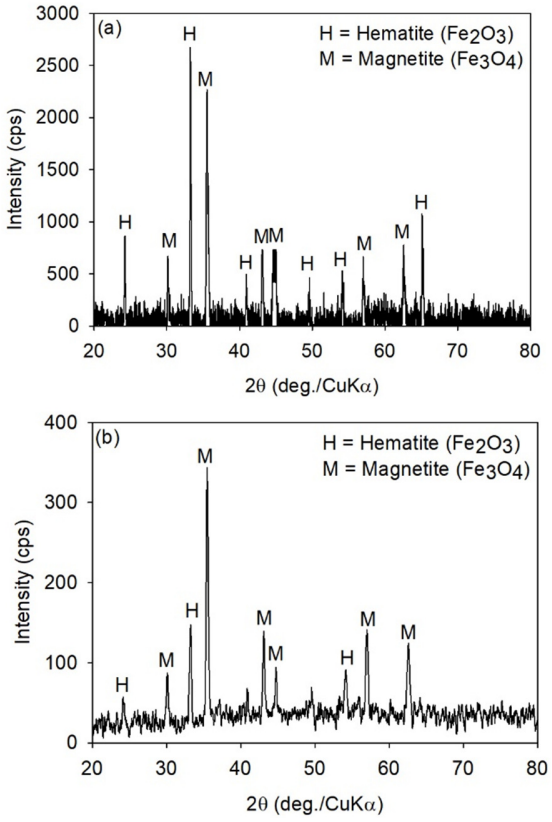

Fig. 2. XRD patterns on oxidized hot-rolled steel established from: (a) medium slab, (b) thin slab.

Figure 4 shows the mass gain after being exposed to water vapor at 600-900 °C for 30, 60, and 90 min. The oxidation behavior of the tested steels was discovered to follow a linear-parabolic rate law. The oxidation of steel is a function of temperature. From the obtained experimental results, the steel established from a medium slab exhibited significantly less oxidation than the steel established from a thin slab. Furthermore, the studied steels during the initial stage seemed to be identical except for the steel made from a thin slab oxidized at 900 °C. It seems that the steel will undergo three stages of oxidation. The initial stage of oxidation followed a linear law which shows that surface reactions predominate in the early stages of oxidation. The oxidation rates in the second stage correspond to the parabolic law. This duration might be related to the formation of the protective SiO_2 layer. The oxidation rates in the third stage, which exhibit a higher parabolic rate constant, also follow a parabolic law. It is believed that during this time, the protective SiO_2 layer changed into a less protective layer composed of wustite and fayalite. However, the mass gain of steel oxidized at 600 °C for 40 or 60 min tends to decrease compared to other conditions. It might then be noted that the mass gain of steel was typically much lower and the oxidation rate decreased due to the gradual loss of contact between the oxide scale and the substrate at 600 °C. The duration in which the oxidation behavior was linear in steel established from a medium slab increased by adding more Si to the steel. This indicates that the primary diffusing defect was the hydroxyl ion. The growth rate of the p-type external oxide was slowed by increasing the Si content. As a result, the diffusion rate of the hydroxyl ions along the grain boundaries was faster than the rate of the surface reaction for a longer period of time. During the parabolic oxidation, the oxidation rate of the steel established from a medium slab was higher than that of the steel established from a thin slab. The oxidation rate for forming the internal subscale increases when the silicon content of the steel increases. The main cause of this was the increased fayalite production given by the higher Si content. Moreover, the higher Si content in the steel may make it simpler for hydroxyl ions to diffuse along the grain boundaries.

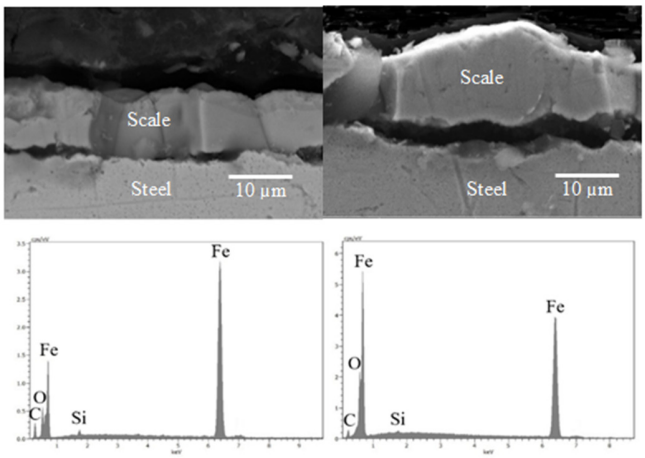

Fig. 3. SEM cross sections and EDS patterns focusing on the scale-steel interface of steel established from medium slab (left) and from thin slab (right) oxidized in 20%H_2O-80%N_2.

The parabolic rate constants (k_p) can be used to compare the oxidation rates of the two studied steels. The energy needed to initiate a chemical reaction can be described by the Arrhenius plot with regard to activation energy. Using information from

Table III, the Arrhenius plot depicting a correlation between the parabolic rate constant and temperature is presented in Figure 5. The oxidation rate of steel established from medium slabs was found to be lower than that of steel established from thin slabs. The parabolic rate constant is shown in (5) for steel established from a medium slab and (6) for steel established from a thin slab. Information obtained from Figure 5 is listed in Table IV.

TABLE III. PARABOLIC RATE CONSTANTS OF TWO STUDIES HOT-ROLLED STEEL OXIDIZED IN 20%H_2O-N_2

Temperature (°C)	Parabolic rate constant k_p ($g^2.cm^{-4}.s^{-1}$)	
	Steel made from medium slab	Steel made from thin slab
600	$3.01 \times 10^{-8} \pm 5.09 \times 10^{-9}$	$2.44 \times 10^{-8} \pm 1.09 \times 10^{-9}$
700	$3.69 \times 10^{-8} \pm 3.09 \times 10^{-9}$	$1.16 \times 10^{-7} \pm 1.02 \times 10^{-8}$
800	$5.91 \times 10^{-8} \pm 2.09 \times 10^{-8}$	$4.16 \times 10^{-7} \pm 4.55 \times 10^{-8}$
900	$5.78 \times 10^{-7} \pm 3.09 \times 10^{-7}$	$6.83 \times 10^{-7} \pm 6.89 \times 10^{-8}$

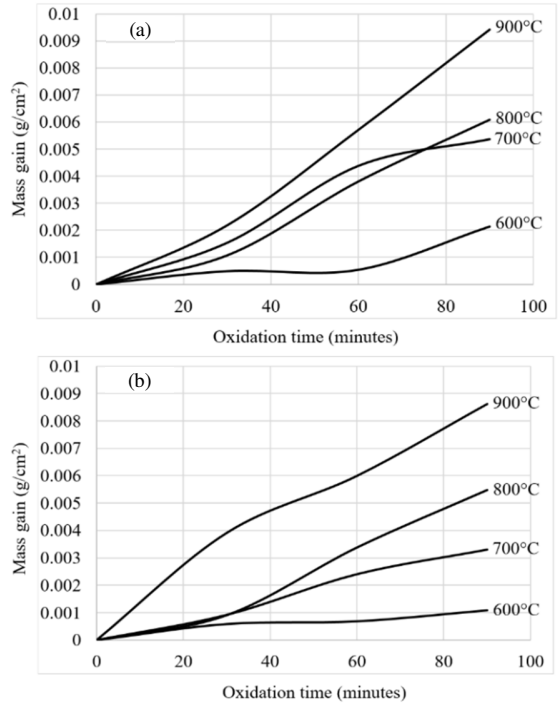

Fig. 4. Mass gain curves of steel established from: (a) a medium slab, (b) a thin slab, oxidized in water vapor at different temperatures.

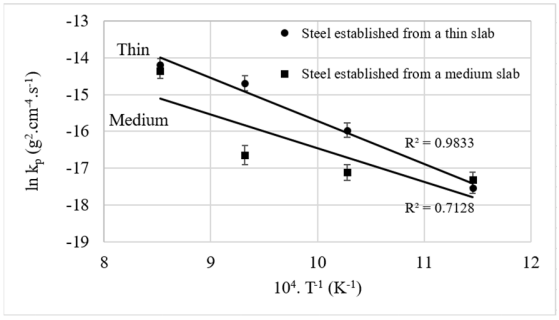

Fig. 5. Arrhenius plot of the rate constant k_p for the oxidation kinetics of hot-rolled steel established from medium and thin slabs.

$$k_p = 15.12e^{-\frac{174088}{RT}} \quad (5)$$

$$k_p = 14.00e^{-\frac{223827}{RT}} \quad (6)$$

where k_p represents the parabolic rate constant ($g^2.cm^{-4}.s^{-1}$), R represents the gas constant (8.314 $J.mol^{-1}.K^{-1}$), and T represents the temperature (K). The hot-rolled steel established from medium and thin slabs had apparent activation energies of 174 and 224 $kJ.mol^{-1}$, respectively.

TABLE IV. MEASURED PARAMETERS OF THE TWO STUDIED HOT-ROLLED STEELS FROM ARRHENIUS PLOT

Parameters	Steel made from medium slab	Steel made from thin slab
Slope (m)	-0.91	-1.17
Proportional constant k_o ($g^2.cm^{-4}.s^{-1}$)	-15.12	-14.00
Apparent activation energies E_a ($J.mol^{-1}$)	174088	223827

It was found from the results that when the silicon content increased in steel established from medium slabs, it tended to reduce the oxidation rate. The SEM-EDS revealed that the interfacial layer of steel established from a medium slab has an oxide with a higher Si content than the steel established from a thin slab. This was caused by a Si-enriched oxide that was present at the steel-scale interface and increased the steel passivity as the fayalite phase was produced. The production of external oxide was obstructed by the presence of the internal subscale formed by fayalite. The lower oxidation rate of external oxide formation was more prominent than the oxidation rate of internal oxide formation. The lower scale thickness and mass gain decreased as Si increased. Regarding the commercial application, if the hot-rolled steel was provided for further cold rolling, prior to the cold rolling process, the oxide scale is entirely eliminated. Hot-rolled steel established from a medium slab has a thinner oxide scale than the steel established from a thin slab, thus scale removal would be simple. However, scale adhesion must be further considered.

IV. CONCLUSTION

In this paper, hot-rolled steel with different Si contents established from medium and thin slabs was studied in paper. The oxidation behavior of steel was the main focus of this research. The steel was oxidized in a horizontal furnace with a 20% H_2O-N_2 atmosphere at a temperature of 600-900 °C for 30, 60, and 90 min. The result showed that the oxidation rate of the studied steel obeyed the linear and parabolic law. Oxide compounds primarily involve oxygen from water vapor. Hematite and magnetite can be produced from water vapor under the oxidation condition that was released into the atmosphere under the P_{H_2O}/P_{H_2} ratio. The overall oxidation rate was slowed by alloying the steel with Si. This was due to the internal subscale as fayalite propensity to prevent iron from steel for diffusing outwardly and forming the external scale. The protective layer of Si-containing oxide at the steel-scale interface tends to be promoted by an increase in silicon content in steel established from medium slab. This layer was exhibited

as a barricade of Fe ions to form oxide layers, which corresponded to a lower oxidation rate in the steel.

ACKNOWLEDGMENT

This research was funded by King Mongkut's University of Technology, North Bangkok, Contract no. KMUTNB-64-DRIVE-35. G Steel Public Company Limited is acknowledged for the provision of the hot-rolled steel strips.

REFERENCES

[1] A. Ghosh and A. Chatterjee, *Iron Making and Steelmaking: Theory and Practice*. New Delhi, India: PHI Learning, 2008.

[2] V. B. Ginzburg, *Flat-Rolled Steel Processes: Advanced Technologies*. New York, NY, USA: CRC Press, 2009.

[3] R. Y. Chen and W. Y. D. Yeun, "Review of the High-Temperature Oxidation of Iron and Carbon Steels in Air or Oxygen," *Oxidation of Metals*, vol. 59, no. 5, pp. 433–468, Jun. 2003, https://doi.org/10.1023/A:1023685905159.

[4] K. Ngamkham, N. Klubvihok, J. Tungtrongpairoj, and S. Chandra-Ambhorn, "Relationship between entry temperature and properties of thermal oxide scale on low carbon steel strips," in *14th International Conference on Metal forming*, Krakow, Poland, Sep. 2012, pp. 991–994.

[5] S. Chandra-ambhorn, K. Ngamkham, and N. Jiratthanakul, "Effects of Process Parameters on Mechanical Adhesion of Thermal Oxide Scales on Hot-Rolled Low Carbon Steels," *Oxidation of Metals*, vol. 80, no. 1, pp. 61–72, Aug. 2013, https://doi.org/10.1007/s11085-013-9370-6.

[6] R. Y. Chen and W. Y. D. Yuen, "Oxide-Scale Structures Formed on Commercial Hot-Rolled Steel Strip and Their Formation Mechanisms," *Oxidation of Metals*, vol. 56, no. 1, pp. 89–118, Aug. 2001, https://doi.org/10.1023/A:1010395419981.

[7] L. Suarez, R. H. Petrov, L. A. I. Kestens, M. Lamberigts, and Y. Houbaert, "Texture Evolution of Tertiary Oxide Scale during Steel Plate Finishing Hot Rolling Simulation Tests," *Materials Science Forum*, vol. 550, pp. 557–562, 2007, https://doi.org/10.4028/www.scientific.net/MSF.550.557.

[8] P. Sarrazin, A. Galerie, and J. Fouletier, *Mechanisms of High Temperature Corrosion*. Zurich, Switzerland: Trans Tech Publications, 2008.

[9] T. Nilsonthi, J. Tungtrongpairoj, S. Chandra-Ambhorn, Y. Wouters, and A. Galerie, "Effect of silicon on formation and mechanical adhesion of thermal oxide scale grown on low carbon steels in a hot-rolling line," in *14th International Conference on Metal forming*, Krakow, Poland, Sep. 2012, pp. 987–990.

[10] T. Nilsonthi, S. Chandra-ambhorn, Y. Wouters, and A. Galerie, "Adhesion of Thermal Oxide Scales on Hot-Rolled Conventional and Recycled Steels," *Oxidation of Metals*, vol. 79, no. 3, pp. 325–335, Apr. 2013, https://doi.org/10.1007/s11085-012-9356-9.

[11] S. Chandra-ambhorn, T. Nilsonthi, Y. Wouters, and A. Galerie, "Oxidation of simulated recycled steels with 0.23 and 1.03wt.% Si in Ar–20%H2O at 900°C," *Corrosion Science*, vol. 87, pp. 101–110, Oct. 2014, https://doi.org/10.1016/j.corsci.2014.06.018.

[12] M. I. Mohamed, "Studies of the Properties and Microstructure of Heat Treated 0.27% C and 0.84% Mn Steel," *Engineering, Technology & Applied Science Research*, vol. 8, no. 5, pp. 3484–3487, Oct. 2018, https://doi.org/10.48084/etasr.2065.

[13] K. Touileb, A. Hedhibi, R. Djoudjou, A. Ouis, and M. L. Bouazizi, "Mixing Design for ATIG Morphology and Microstructure Study of 316L Stainless Steel," *Engineering, Technology & Applied Science Research*, vol. 9, no. 2, pp. 3990–3997, Apr. 2019, https://doi.org/10.48084/etasr.2665.

[14] I. H. Kara, T. A. I. Yousef, H. Ahlatci, and Y. Turen, "Ca and Ce Effect on the Corrosion Resistance of Hot-Rolled AZ31 Mg Alloys," *Engineering, Technology & Applied Science Research*, vol. 10, no. 1, pp. 5113–5116, Feb. 2020, https://doi.org/10.48084/etasr.3238.

[15] W. Wongpromrat, H. Thaikan, W. Chandra-ambhorn, and S. Chandra-ambhorn, "Chromium Vaporisation from AISI 441 Stainless Steel Oxidised in Humidified Oxygen," *Oxidation of Metals*, vol. 79, no. 5, pp. 529–540, Jun. 2013, https://doi.org/10.1007/s11085-013-9379-x.

[16] P. Promdirek, G. Lothongkum, S. Chandra-Ambhorn, Y. Wouters, and A. Galerie, "Oxidation Kinetics of AISI 441 Ferritic Stainless Steel at High Temperatures in CO2 Atmosphere," *Oxidation of Metals*, vol. 81, no. 3, pp. 315–329, Apr. 2014, https://doi.org/10.1007/s11085-013-9432-9.

[17] W. Wongpromrat *et al.*, "Possible connection between nodule development and presence of niobium and/or titanium during short time thermal oxidation of AISI 441 stainless steel in wet atmosphere," *Materials at High Temperatures*, vol. 32, no. 1–2, pp. 22–27, Jan. 2015, https://doi.org/10.1179/0960340914Z.00000000057.

[18] A. Atkinson, "Transport processes during the growth of oxide films at elevated temperature," *Reviews of Modern Physics*, vol. 57, no. 2, pp. 437–470, Apr. 1985, https://doi.org/10.1103/RevModPhys.57.437.

[19] D. Landolt, *Corrosion et chimie de surfaces des metaux*, Reimp. corr. Lausanne, Switzerland: PPUR Press, 1997.

[20] P. Kofstad, *High temperature corrosion*. London, UK: Elsevier, 1988.

[21] M. J. L. Gines, G. J. Benitez, T. Perez, E. Merli, M. A. Firpo, and W. EgliI, "Study of the picklability of 1.8 mm hot-rolled steel strip in hydrochloric acid," *Latin American applied research*, vol. 32, no. 4, pp. 281–288, Dec. 2002.

[22] Z. Y. Jiang, A. K. Tieu, W. H. Sun, J. N. Tang, and D. B. Wei, "Characterisation of thin oxide scale and its surface roughness in hot metal rolling," *Materials Science and Engineering: A*, vol. 435–436, pp. 434–438, Nov. 2006, https://doi.org/10.1016/j.msea.2006.07.070.

[23] M. Zhang and G. Shao, "Characterization and properties of oxide scales on hot-rolled strips," *Materials Science and Engineering: A*, vol. 452–453, pp. 189–193, Apr. 2007, https://doi.org/10.1016/j.msea.2006.10.151.

[24] Y.-L. Yang, C.-H. Yang, S.-N. Lin, C.-H. Chen, and W.-T. Tsai, "Effects of Si and its content on the scale formation on hot-rolled steel strips," *Materials Chemistry and Physics*, vol. 112, no. 2, pp. 566–571, Dec. 2008, https://doi.org/10.1016/j.matchemphys.2008.06.021.

[25] A. Segawa, "Reproduction and Deformation Characteristics of Oxide Scale in Hot Rolling Using Vacuum Rolling Mill," *Materials Science Forum*, vol. 696, pp. 150–155, 2011, https://doi.org/10.4028/www.scientific.net/MSF.696.150.

[26] S. Taniguchi, K. Yamamoto, D. Megumi, and T. Shibata, "Characteristics of scale/substrate interface area of Si-containing low-carbon steels at high temperatures," *Materials Science and Engineering: A*, vol. 308, no. 1, pp. 250–257, Jun. 2001, https://doi.org/10.1016/S0921-5093(00)01977-8.

[27] T. Ishitsuka, Y. Inoue, and H. Ogawa, "Effect of Silicon on the Steam Oxidation Resistance of a 9%Cr Heat Resistant Steel," *Oxidation of Metals*, vol. 61, no. 1, pp. 125–142, Feb. 2004, https://doi.org/10.1023/B:OXID.0000016280.81734.3f.

[28] M. Takeda and T. Onishi, "Oxidation Behavior and Scale Properties on the Si Containing Steels," *Materials Science Forum*, vol. 522–523, pp. 477–488, 2006, https://doi.org/10.4028/www.scientific.net/MSF.522-523.477.

[29] T. Nishimoto, K. Honda, Y. Kondo, and K. Uemura, "Effects of Si Content on the Oxidation Behavior of Fe–Si Alloys in Air," *Materials Science Forum*, vol. 696, pp. 126–131, 2011, https://doi.org/10.4028/www.scientific.net/MSF.696.126.

[30] E. Ahtoy, "Effect of alloying elements (Si, P, Al, B) on low carbon steel oxidation in process at high temperatures mechanisms and modelling," Ph.D. dissertation, Grenoble INPG, Grenoble, France, 2010.

[31] R. Y. Chen and W. Y. D. Yuen, "Effects of the Presence of Water Vapour on the Oxidation Behaviour of Low Carbon–Low Silicon Steel in 1 %O2–N2 at 1073 K," *Oxidation of Metals*, vol. 79, no. 5, pp. 655–678, Jun. 2013, https://doi.org/10.1007/s11085-012-9314-6.

[32] R. Y. Chen and W. Y. D. Yuen, "Effects of the Presence of Water Vapour on the Oxidation Behaviour of Low Carbon–Low Silicon Steel in 1 %O2–N2 at 1,173 and 1,273 K," *Oxidation of Metals*, vol. 79, no. 5, pp. 679–699, Jun. 2013, https://doi.org/10.1007/s11085-013-9377-z.

[33] R. Y. Chen and W. Y. D. Yuen, "Longer Term Oxidation Kinetics of Low Carbon, Low Silicon Steel in 17H2O–N2 at 900°C," *Oxidation of*

Metals, vol. 85, no. 5, pp. 489–507, Jun. 2016, https://doi.org/10.1007/s11085-016-9608-1.

[34] D. R. Gaskell, *Introduction to metallurgical thermodynamics*, 2nd ed. New York, NY, USA: McGraw-Hill, 1981.

[35] R. Y. Chen and W. Y. D. Yuen, "Oxidation of Low-Carbon Steel in 17H2O-N2 at 900 °C," *Metallurgical and Materials Transactions A*, vol. 40, no. 13, pp. 3091–3107, Dec. 2009, https://doi.org/10.1007/s11661-009-0049-1.